Near-field channel reconstruction and user location for ELAA systems

Lu, Z., Han, Y., Jin, S., Matthaiou, M., & Quek, T. Q. S. (2022). Near-field channel reconstruction and user location for ELAA systems. In *Proceedings: 2022 IEEE International Symposium on Wireless Communications Systems (ISWCS)* (International Symposium on Wireless Communication Systems (ISWCS): Proceedings). Institute of Electrical and Electronics Engineers Inc.. https://doi.org/10.1109/ISWCS56560.2022.9940362

Published in:
Proceedings: 2022 IEEE International Symposium on Wireless Communications Systems (ISWCS)

Document Version:
Peer reviewed version

Near-Field Channel Reconstruction and User Location for ELAA Systems

Zhizheng Lu*, Yu Han*†, Shi Jin*, Michail Matthaiou§, and Tony Q. S. Quek†
*National Mobile Communications Research Laboratory, Southeast University, Nanjing, China
†Information System Technology and Design Pillar, Singapore University of Technology and Design, Singapore
§Centre for Wireless Innovation (CWI), Queen's University Belfast, BT3 9DT, Belfast, U.K
E-mail: {luzz, hanyu, jinshi}@seu.edu.cn, m.matthaiou@qub.ac.uk, tonyquek@sutd.edu.sg

***Abstract*—In this paper, we propose an efficient near-field channel reconstruction and user localization scheme for extremely large-scale antenna array (ELAA) systems. Due to the non-negligible near-field effect in ELAA systems, a more realistic near-field multipath channel model, which incorporates the unequal path loss and the phase deviations across antennas and models line-of-sight (LoS), reflection, and scattering, is considered. A subarray hybrid beamforming architecture is further employed to reduce the cost of using ELAA. Based on the sparsity of the near-field channel in the joint angle-distance domain, a near-field Newtonized orthogonal matching pursuit algorithm is proposed to estimate the multipath parameters. Reconstruction of the near-field channel and positioning of the user can be achieved based on the estimated parameters. Our numerical results verify that the reconstructed channel is very close to the real near-field channel, and the user localization has high accuracy whether a LoS component exists or not, validating the effectiveness and reliability of the proposed scheme.**

I. Introduction

Massive multiple-input multiple-output (MIMO) is an enabling technology for the current fifth generation (5G) mobile communication systems, playing a key role in improving the spectral efficiency [1]. With the development of the sixth generation (6G) systems, the need for higher spectral and energy efficiencies becomes indispensable, which will require a further increase in the number of antennas at the base station (BS) [2]. ELAA systems are equipped with a much larger number of antennas at the BS than massive MIMO, and can achieve multifold improvement in the achievable spectral efficiency [3]. In addition, with the gradual penetration of millimeter wave and THz technologies, wireless systems can avail of extremely high spectrum resources. Equally importantly, the size of antenna elements can be made very small at high-frequency bands [4], which makes it possible to pack an extremely large number of antennas in a limited area. Therefore, ELAA technology has a promising development and application potential in the future 6G era.

Due to the high cost of high-frequency radio frequency (RF) chains [5], ELAA systems may utilize a subarray hybrid precoding architecture at the BS. The number of RF chains is much smaller than the number of antennas, and, thus, a large pilot overhead will be needed for channel estimation in ELAA systems. Much work has been done to study how to estimate CSI with low pilot overhead. In traditional MIMO systems, based on the sparse feature of the channel in the angular domain, compressed sensing (CS) algorithms can be used to estimate the uplink CSI through uplink pilot training. For example, [6] and [7] considered the plane wave-front channel model and utilized the Newtonized orthogonal matching pursuit (NOMP) algorithm to estimate the uplink channel parameters. Due to the nonnegligible curvature characteristic of the channel in the near field, [8] modeled the channel with spherical wavefronts and the real phase deviations among the antenna array were also considered. However, there are very few related works studying the near-field channel reconstruction and user localization considering the real phase and amplitude deviations across the receiving antennas.

In this study, we consider a more realistic near-field multipath channel model, which incorporates the unequal path loss and the phase deviations across the receiving antennas based on the spherical wavefront model. The LoS, reflection, and scattering manifestations are also modeled in the channel. A near-field Newtonized orthogonal matching pursuit [9] (N-NOMP) algorithm is proposed for the subarray hybrid precoding based ELAA system to estimate the multipath channel parameters. Specifically, a two-dimensional joint angle-distance domain dictionary is designed, and a stopping threshold is derived without the knowledge of the number of paths. Utilizing N-NOMP, near-field channel reconstruction and user localization can be realized with limited training overhead. Simulations are conducted to evaluate the normalized mean square error (NMSE) performance of the proposed channel reconstruction and user localization scheme. The results demonstrate that the near-field channel can be reconstructed accurately in a wide signal to noise ratio (SNR) range, while the user position can be detected precisely.

II. System Model

We consider a single cell ELAA mobile communication narrowband system which employs a subarray hybrid precoding architecture at the BS. Time division duplexing is applied. The carrier frequency is denoted as f_c. The carrier wavelength is $\lambda_c = \frac{c}{f_c}$, where c denotes the speed of light. As shown in Fig. 1, the BS is equipped with an N-antennas uniform linear array and N_{RF} radio frequency (RF) chains, satisfying $N_{\mathrm{RF}} \ll N$. We assume that N is an integer multiple of N_{RF},

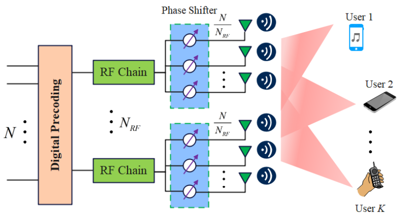

Fig. 1. ELAA system model with subarray architecture.

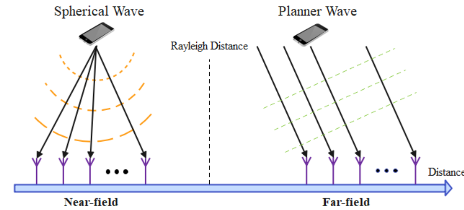

Fig. 2. Near-field and far-field signal model.

and each RF chain is connected to $\frac{N}{N_{\mathrm{RF}}}$ antennas through phase shifters. The spacing between adjacent antennas is $d = \frac{\lambda_c}{2}$. The mobile user has a single antenna, while T is defined as the number of pilots. We denote the t-th transmit pilot as x_t. Hence, the received pilot $\mathbf{y}_t \in \mathbb{C}^{N_{\mathrm{RF}} \times 1}$ can be expressed as

$$\mathbf{y}_t = \mathbf{A}_t \mathbf{h} x_t + \mathbf{A}_t \mathbf{z}_t, \tag{1}$$

where $\mathbf{A}_t \in \mathbb{C}^{N_{\mathrm{RF}} \times N}$ denotes the constant modulus analog combining matrix satisfying

$$|\mathbf{A}_t (i,j)| = \begin{cases} 1, & j = \frac{(i-1)N}{N_{\mathrm{RF}}} + 1, \ldots, \frac{iN}{N_{\mathrm{RF}}} \\ 0, & \text{else} \end{cases}, \tag{2}$$

for $i = 1, \ldots, N_{\mathrm{RF}}$, while the phase follows a uniform distribution within $[0, 2\pi]$. Note that $\mathbf{h} \in \mathbb{C}^{N \times 1}$ denotes the real near-field uplink channel vector. The additive Gaussian complex noise $\mathbf{z}_t \in \mathbb{C}^{N \times 1}$ follows the distribution $\mathcal{CN}\left(0, \sigma^2 \mathbf{I}_N\right)$. We assume that the transmit signal is $x_t = \sqrt{P}$ for $t = 1, \ldots, T$, where the transmitted power equals P. All the received pilots can be stacked together and written as

$$\mathbf{y} = \sqrt{P} \mathbf{A} \mathbf{h} + \mathbf{n}, \tag{3}$$

where $\mathbf{A} = \left[\mathbf{A}_1^{\mathrm{T}}, \cdots, \mathbf{A}_T^{\mathrm{T}}\right]^{\mathrm{T}} \in \mathbb{C}^{T N_{\mathrm{RF}} \times N}$ denotes the overall analog combining matrix for all pilots, while $(\cdot)^{\mathrm{T}}$ denotes the transpose. Similarly, $\mathbf{n} = \left[\mathbf{n}_1^{\mathrm{T}} \mathbf{A}_1^{\mathrm{T}}, \cdots, \mathbf{n}_T^{\mathrm{T}} \mathbf{A}_T^{\mathrm{T}}\right]^{\mathrm{T}}$ denotes the noise after analog combining.

Due to the extra large aperture of the array, which equals $(N-1)d$ here, users may not be in the far-field region of the array, causing non-negligible amplitude and phase deviations of the channel across the array as shown in Fig. 2. When the distance between a user and array is greater than the Rayleigh distance $d_{\mathrm{R}} = \frac{2((N-1)d)^2}{\lambda_c}$, the amplitude and phase deviation can be ignored, and the user is in the far-field region. For example, $d_{\mathrm{R}} = 325.125$ meters for $N = 256$ and $f_c = 30$ GHz. Notably, if the distance is less than d_{R}, the amplitude and phase variations of the channel across the ELAA are large and can no longer be ignored in the near-field. Hence, instead of the traditional far-field channel model, the near-field channel model should be considered here.

As shown in Fig. 3, we set the central antenna of the BS array as the reference antenna and make it as the origin of the coordinate system. A large smooth surface exists near the BS, providing a strong reflection path in the user channel. The smooth wall is orthogonal to the array, and its center is $\left(\frac{W}{2}, \frac{(N-1)d}{2} + S\right)$, where S denotes the vertical distance between the first antenna at the BS and the smooth surface; W denotes the length of the smooth wall. Assuming that the user location is (x, y), the location of the image of the user is $(x, -y + (N-1)d + 2S)$. By transforming the Cartesian system to the polar system, the near-field channel can be modeled as

$$\mathbf{h} = \sum_{l=1}^{L} g_l \mathbf{c}(\theta_l, r_l) \odot \mathbf{b}(\theta_l, r_l), \tag{4}$$

where L denotes the number of paths between the user and the BS; g_l is the complex gain between the user and the reference antenna; r_l denotes the distance from the user, the scatterer or the smooth surface to the transmitter in the l-th path; $\theta_l = \cos(\varphi_l)$ refers to the cosine of the angle of arrival (AoA) φ_l at the reference antenna as shown in Fig. 3. Also, $\mathbf{c}(\theta_l, r_l)$ and $\mathbf{b}(\theta_l, r_l)$ are the gain correction vector and the phase correction vector, which model the gain and phase deviations between the reference antenna and other antennas at the BS, respectively. Note that $\odot$ denotes the Hadamard product. The gain correction vector $\mathbf{c}(\theta_l, r_l)$ can be written as

$$\mathbf{c}(\theta_l, r_l) = \left[\frac{r_l}{r_{l,1}}, \ldots, \frac{r_l}{r_{l,N}}\right]^{\mathrm{T}}, \tag{5}$$

where $r_{l,n}$ denotes the real distance from the scatterer to the n-th receiving antenna at the BS in the l-th path, i.e.,

$$r_{l,n} = \sqrt{r_l^2 - 2\delta_n r_l d \theta_l + \delta_n^2 d^2}, \tag{6}$$

where $\delta_n = \frac{2n-N-1}{2}$ for $n = 1, \ldots, N$. Similarly, the phase correction vector $\mathbf{b}(\theta_l, r_l)$ can be written as

$$\mathbf{b}(\theta_l, r_l) = \left[e^{jk_c(r_{l,1} - r_l)}, \ldots, e^{jk_c(r_{l,N} - r_l)}\right]^{\mathrm{T}}, \tag{7}$$

where $k_c = \frac{2\pi f_c}{c}$. Notably, the L paths may be composed of a LoS path, a reflected path, and $L-2$ NLoS paths caused by scatterers, or, a reflected path and $L-1$ NLoS scattering paths. If the LoS path exists, it is set as the first and strongest path of the channel, and the reflected path as the second path whose gain is lower than that of the LoS path but stronger than any NLoS scattering path. The LoS path $\mathbf{h}_{\mathrm{LoS}}$ can be written as

$$\mathbf{h}_{\mathrm{LoS}} = \xi \frac{\lambda_c}{4\pi r_{\mathrm{LoS}}} e^{-jk_c r_{\mathrm{LoS}}} \mathbf{c}(\theta_{\mathrm{LoS}}, r_{\mathrm{LoS}}) \odot \mathbf{b}(\theta_{\mathrm{LoS}}, r_{\mathrm{LoS}}). \tag{8}$$

Note that when LoS exists, $\xi = 1$, otherwise $\xi = 0$; θ_{LoS} and r_{LoS} respectively represent the cosine of the AoA and the

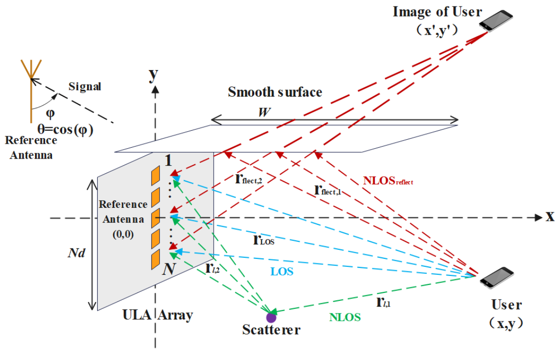

Fig. 3. Near-field channel model.

distance from the user to the reference antenna. The reference complex gain is $g_1 = \xi \frac{\lambda_c}{4\pi r_{\text{LoS}}} e^{-jk_c r_{\text{LoS}}}$. The smooth surface can be approximated as a mirror. Then, the path reflected by the smooth surface can be seen as the LoS path between the user's mirror image and the BS. The reflection path $\mathbf{h}_{\text{ref}}$ can be expressed as [3]

$$\mathbf{h}_{\text{ref}} = \frac{\alpha \lambda_c}{4\pi r_{\text{ref}}} e^{-jk_c r_{\text{ref}}} \mathbf{c}\left(\theta_{\text{ref}}, r_{\text{ref}}\right) \odot \mathbf{b}\left(\theta_{\text{ref}}, r_{\text{ref}}\right), \tag{9}$$

where $r_{\text{ref}} = r_{\text{ref},1} + r_{\text{ref},2}$; $|\alpha| \in (0,1)$ models the degradation of gain due to reflection; $r_{\text{ref},1}$ and $r_{\text{ref},2}$ respectively denote the distance from the user to the smooth surface and the distance from the smooth surface to the reference antenna; θ_{ref} denotes the cosine of the AoA from the image of the user to the reference antenna. The reference complex gain is $g_2 = \frac{\alpha \lambda_c}{4\pi r_{\text{ref}}} e^{-jk_c r_{\text{ref}}}$. The NLoS components can be written as [10]

$$\mathbf{h}_{\text{NLoS}} = \sum_{l=3}^{L} \frac{\beta \lambda_c^2}{(4\pi)^2 r_{l,1} r_{l,2}} e^{-jk_c (r_{l,1}+r_{l,2})} \mathbf{c}\left(\theta_l, r_{l,2}\right) \odot \mathbf{b}\left(\theta_l, r_{l,2}\right), \tag{10}$$

where $|\beta| \in (0,1)$ describes the reflectivity of the scatterers; $r_{l,1}$ is the distance from the user to the scatterer and $r_{l,2}$ is the distance from the scatterer to the reference antenna in the l-th path. The reference gains are $g_l = \frac{\beta \lambda_c^2}{(4\pi)^2 r_{l,1} r_{l,2}} e^{-jk_c (r_{l,1}+r_{l,2})}$ for $l = 3, \ldots, L$ and satisfy $|g_l| \ll |g_2| < |g_1|$.

In this paper, we focus on the near-field channel reconstruction and localization problem in the subarray hybrid precoding ELAA system given a limited amount of received pilots in (3). The channel model can be further simplified as

$$\mathbf{h} = \sum_{l=1}^{L} g_l \mathbf{w}\left(\theta_l, r_l\right), \tag{11}$$

where the gain-phase joint correction vector is $\mathbf{w}(\theta_l, r_l) = \mathbf{c}(\theta_l, r_l) \odot \mathbf{b}(\theta_l, r_l)$. That is, the near-field channel model can be simplified as the weighted sum of equivalent correction vectors, which experiences sparsity in the joint angle-distance domain. Sparse channel recovery methods for the far-field scenario can be extended to the near-field CSI estimation.

III. Near-field Channel Estimation And User Location

To realize the reconstruction of near-field channel and user location with low pilot consumption, the N-NOMP algorithm is proposed to estimate the channel parameters, i.e., $(\theta_l, r_l), l = 1, \ldots, L$. N-NOMP is an iterative algorithm and works in the following steps.

A. Whitening Noise

The noise in (3) no longer follows the Gaussian distribution. In order to accurately estimate the channel parameters through the N-NOMP algorithm, a whitening algorithm should be applied firstly to re-whiten the noise. The noise covariance matrix can be expressed as

$$\mathbf{C} = \mathrm{E}\left(\mathbf{n}\mathbf{n}^{\mathrm{H}}\right) = \text{blkdiag}\left(\sigma^2 \mathbf{A}_1 \mathbf{A}_1^{\mathrm{H}}, \ldots, \sigma^2 \mathbf{A}_T \mathbf{A}_T^{\mathrm{H}}\right), \tag{12}$$

where $(\cdot)^{\mathrm{H}}$ denotes the conjugate transpose; $\mathrm{E}(\cdot)$ and $\text{blkdiag}(\cdot)$ denote the expection operation and the block diagonal matrix construction function respectively. We perform the Cholesky factorization of $\mathbf{C} = \sigma^2 \mathbf{D}\mathbf{D}^{\mathrm{H}}$, where $\mathbf{D} \in \mathbb{C}^{TN_{\text{RF}} \times TN_{\text{RF}}}$ is a lower triangular matrix, and the whitening matrix is $\mathbf{D}^{-1}$ [8]. After whitening the noise, the equivalent received pilot $\bar{\mathbf{y}}$ can be rewritten as

$$\bar{\mathbf{y}} = \mathbf{D}^{-1}\mathbf{y} = \mathbf{D}^{-1}\mathbf{A}\mathbf{h} + \bar{\mathbf{n}}. \tag{13}$$

The covariance matrix of $\bar{\mathbf{n}}$ is $\bar{\mathbf{C}} = \mathbf{D}^{-1}\mathbf{C}\mathbf{D}^{-\mathrm{H}} = \sigma^2 \mathbf{I}_{TN_{\text{RF}}}$. Then, the noise has been whitened as Gaussian white noise. Substituting (11) into the equation (13), we can get

$$\bar{\mathbf{y}} = \sum_{l=1}^{L} g_l \mathbf{a}\left(\theta_l, r_l\right) + \bar{\mathbf{n}}, \tag{14}$$

where the equivalent steering vector is $\mathbf{a}(\theta_l, r_l) = \mathbf{D}^{-1}\mathbf{A}\mathbf{w}(\theta_l, r_l)$.

B. N-NOMP Algorithm for Channel Estimation

Since the equivalent received pilot at the BS can be regarded as the weighted sum of the equivalent steering vectors of L paths and the white noise, we extend the NOMP algorithm [9] into the near-field channel condition to estimate the ternary parameter set (g, θ, r) of each path from the noisy sum. A new ternary parameter set $\left(\hat{g}, \hat{\theta}, \hat{r}\right)$ is detected at each iteration, and then the estimated path is removed from the equivalent received pilot. At the end of the $(i-1)$-th iteration, the residual signal can be expressed as

$$\bar{\mathbf{y}}_r = \bar{\mathbf{y}} - \sum_{l=1}^{i-1} \hat{g}_l \mathbf{a}\left(\hat{\theta}_l, \hat{r}_l\right), \tag{15}$$

where $\left(\hat{g}_l, \hat{\theta}_l, \hat{r}_l\right)$ for $l = 1, \ldots, i-1$ represents the ternary parameter set estimated in the previous $i-1$ iterations. In the next i-th iteration, a new ternary parameter set $\left(\hat{g}_i, \hat{\theta}_i, \hat{r}_i\right)$ is estimated by minimizing the residual power $\left\|\bar{\mathbf{y}}_r - \hat{g}_i \mathbf{a}\left(\hat{\theta}_i, \hat{r}_i\right)\right\|^2$.

This process is equivalent to maximizing the following equation

$$\mathrm{J}\left(\hat{g}_i, \hat{\theta}_i, \hat{r}_i\right) = 2\mathrm{Re}\left\{\bar{\mathbf{y}}_r^{\mathrm{H}} \hat{g}_i \mathbf{a}\left(\hat{\theta}_i, \hat{r}_i\right)\right\} - |\hat{g}_i|^2 \left\|\mathbf{a}\left(\hat{\theta}_i, \hat{r}_i\right)\right\|^2, \tag{16}$$

where $\bar{\mathbf{y}}_r$ is treated as a constant. Without loss of generality, the iteration number subscript i is omitted in the following sections. The steps of the N-NOMP algorithm in an iteration are the following.

1) New ternary parameter set detection: For any given θ and r, the equivalent reference complex gain $\hat{g}$ can be obtained by maximizing $\mathrm{J}(g, \theta, r)$ as following

$$\hat{g} = \left(\mathbf{a}(\theta, r)^{\mathrm{H}} \bar{\mathbf{y}}_r\right) \Big/ \|\mathbf{a}(\theta, r)\|^2. \tag{17}$$

Substituting $\hat{g}$ back into $\mathrm{J}(g, \theta, r)$, the generalized likelihood ratio test estimate of θ and r can be obtained by

$$\left(\hat{\theta}, \hat{r}\right) = \arg\max_{\theta, r \in \Psi} G_{\bar{\mathbf{y}}_r}(\theta, r), \tag{18}$$

where the cost function is

$$G_{\bar{\mathbf{y}}_r}(\theta, r) = \left|\mathbf{a}(\theta, r)^{\mathrm{H}} \bar{\mathbf{y}}_r\right|^2 \Big/ \|\mathbf{a}(\theta, r)\|^2, \tag{19}$$

where (θ, r) come from the two-dimensional discrete dictionary Ψ. When constructing the discrete dictionary, the angle codebook adopts a uniform sampling form, and the distance codebook adopts an exponential sampling form. The N angle sampling values can be expressed as

$$\left\{\frac{2k_1 - N - 1}{N}, k_1 = 1, \ldots, N\right\}. \tag{20}$$

The channel model is insensitive to distances in the far-field region, and the influence of distance on the received signal can be ignored. Therefore, only the range sampling distances within the Rayleigh distance are considered here. The N distance sampling values can be expressed as

$$\left\{r_{\mathrm{base}}^{k_2}, k_2 = 1, \ldots, N\right\}, \tag{21}$$

where $r_{\mathrm{base}} = d_{\mathrm{R}}^{\frac{1}{N}}$ is the base of the exponential. The two-dimensional discrete dictionary $\Psi(\theta, r)$ can be obtained as

$$\Psi(\theta, r) = \left\{\frac{2k_1 - N - 1}{N}, r_{\mathrm{base}}^{k_2}\right\}, \tag{22}$$

for $k_1 = 1, \ldots, N$, and $k_2 = 1, \ldots, N$.

Then, the coarse estimates of θ and r can be obtained by applying the dictionary $\Psi(\theta, r)$ in (18), and the reference complex gain can be calculated by (17).

2) Single refinement: The N-NOMP algorithm utilizes R_s rounds of the following Newton update steps to refine the coarse estimated parameters. The Newton update step is

$$\begin{bmatrix} \hat{\theta}' \\ \hat{r}' \end{bmatrix} = \begin{bmatrix} \hat{\theta} \\ \hat{r} \end{bmatrix} - \ddot{\mathrm{J}}(g, \theta, r)^{-1} \dot{\mathrm{J}}(g, \theta, r), \tag{23}$$

where

$$\dot{\mathrm{J}}(g, \theta, r) = \begin{bmatrix} \frac{\partial \mathrm{J}}{\partial \theta} \\ \frac{\partial \mathrm{J}}{\partial r} \end{bmatrix}, \tag{24}$$

is the first partial derivative matrix of $\mathrm{J}(g, \theta, r)$, and

$$\ddot{\mathrm{J}}(g, \theta, r) = \begin{bmatrix} \frac{\partial^2 \mathrm{J}}{\partial \theta^2} & \frac{\partial^2 \mathrm{J}}{\partial \theta \partial r} \\ \frac{\partial^2 \mathrm{J}}{\partial r \partial \theta} & \frac{\partial^2 \mathrm{J}}{\partial r^2} \end{bmatrix}, \tag{25}$$

is the second partial derivative matrix of $\mathrm{J}(g, \theta, r)$. Due to the equation $\mathbf{a}(\theta, r) = \mathbf{D}^{-1}\mathbf{A}\mathbf{w}(\theta, r)$, where $\mathbf{D}^{-1}\mathbf{A}$ is independent of θ and r, the first partial derivative can be obtained as

$$\frac{\partial \mathrm{J}}{\partial x} = 2\mathrm{Re}\left\{g(\bar{\mathbf{y}}_r - g\mathbf{a})^{\mathrm{H}} \mathbf{D}^{-1}\mathbf{A} \frac{\partial \mathbf{w}}{\partial x}\right\}, \tag{26}$$

where x can represent θ or r. The second partial derivative can be obtained as

$$\frac{\partial^2 \mathrm{J}}{\partial x_1 \partial x_2} = 2\mathrm{Re}\left\{g(\bar{\mathbf{y}}_r - g\mathbf{a})^{\mathrm{H}} \frac{\partial^2 \mathbf{a}}{\partial x_1 \partial x_2} - |g|^2 \frac{\partial \mathbf{a}^{\mathrm{H}}}{\partial x_2} \frac{\partial \mathbf{a}}{\partial x_1}\right\}, \tag{27}$$

where x_1 and x_2 can represent θ or r respectively, and $\partial \mathbf{a} = \mathbf{D}^{-1}\mathbf{A}\partial \mathbf{w}$.

We only perform the Newton optimization step when the function is locally concave at $\left(\hat{\theta}, \hat{r}\right)$ (i.e., $\left|\ddot{\mathrm{J}}\left(\hat{g}, \hat{\theta}, \hat{r}\right)\right| \geq 0$ and $\ddot{\mathrm{J}}(1,1) < 0$) and the refinement is accepted only when $G_{\bar{\mathbf{y}}_r}\left(\hat{\theta}', \hat{r}'\right) > G_{\bar{\mathbf{y}}_r}\left(\hat{\theta}, \hat{r}\right)$. Then, the optimization results contribute to the decrease of the overall residual energy.

3) Cyclic refinement: In cyclic refinement, R_c rounds of single refinement are carried out for all the ternary parameter sets which have been estimated in the previous i iterations. The refined ternary parameter sets can be expressed as $\left(\hat{g}_l'', \hat{\theta}_l'', \hat{r}_l''\right)$ for $l = 1, \ldots, i$.

4) Equivalent reference complex gains updating: The equivalent reference complex gains of all estimated paths can be re-estimated through the least square (LS) method as

$$[\hat{g}_1'', \ldots, \hat{g}_i'']^{\mathrm{T}} = \mathbf{M}^{\dagger} \bar{\mathbf{y}}, \tag{28}$$

where $\mathbf{M}^{\dagger}$ represents the pseudo inverse of the coefficient matrix $\mathbf{M}$, which can be expressed as

$$\mathbf{M} = \left[\mathbf{a}\left(\hat{\theta}_1'', \hat{r}_1''\right), \ldots, \mathbf{a}\left(\hat{\theta}_i'', \hat{r}_i''\right)\right]. \tag{29}$$

C. Stopping Criterion

The major challenge faced by the N-NOMP algorithm is that the stopping criterion of the NOMP algorithm is no longer applicable in the near-field. It is necessary to find an appropriate stop criterion to judge when the iterative process terminates and to estimate the number of paths accurately.

The additional complex Gaussian white noise follows the distribution $|\bar{n}| \sim \mathcal{CN}\left(0, \sigma^2\right)$, and thus the real part and the imaginary part respectively follow the distribution $\mathrm{Re}[\bar{n}] \sim \mathcal{CN}\left(0, \frac{\sigma^2}{2}\right)$ and $\mathrm{Im}[\bar{n}] \sim \mathcal{CN}\left(0, \frac{\sigma^2}{2}\right)$. Hence, $\frac{2\|\bar{\mathbf{n}}\|^2}{\sigma^2}$ follows a Chi-square distribution of $2TN_{\mathrm{RF}}$ degrees of freedom, i.e., $\frac{2\|\bar{\mathbf{n}}\|^2}{\sigma^2} \sim \chi^2(2TN_{\mathrm{RF}})$. When $2TN_{\mathrm{RF}}$ grows large, $\frac{2\|\bar{\mathbf{n}}\|^2}{\sigma^2}$ follows approximately the Gaussian distribution $\mathcal{CN}(2TN_{\mathrm{RF}}, 4TN_{\mathrm{RF}})$. Then, we can get $\|\bar{\mathbf{n}}\|^2 \sim \mathcal{CN}\left(\sigma^2 TN_{\mathrm{RF}}, \sigma^4 TN_{\mathrm{RF}}\right)$.

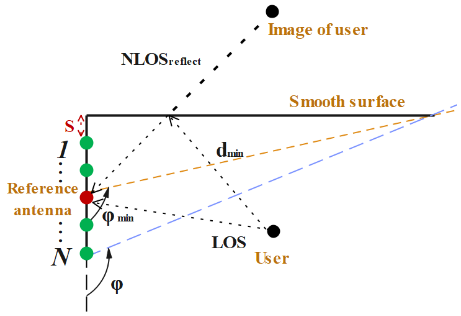

Fig. 4. LOS path existence detection.

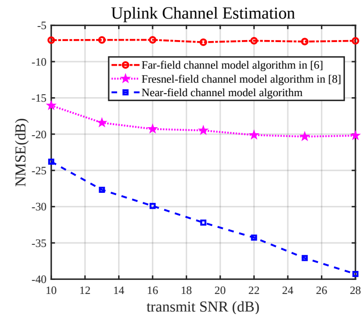

Fig. 5. The NMSE against the SNR ($r_{\rm LOS}=10$ m).

The residual will be reduced to noise (i.e., $\bar{\mathbf{y}}_r \approx \bar{\mathbf{n}}$, $\|\bar{\mathbf{y}}\|^2 \sim \mathcal{CN}\left(\sigma^2 T N_{\rm RF}, \sigma^4 T N_{\rm RF}\right)$) when the N-NOMP algorithm terminates if the ternary parameter set can be estimated accurately, and all the paths can be found. In this paper, the N-NOMP algorithm is designed to terminate when the residual power at the output of the RF chains is less than the noise power. The stopping criterion threshold κ is set to satisfy $\Pr\left\{\|\bar{\mathbf{y}}_r\|^2 > \kappa\right\} = P_{\rm fa}$, where $P_{\rm fa}$ is a nominal false alarm rate, and the stopping criterion threshold can correctly detect the number of paths with $1-P_{\rm fa}$ probability. The threshold can be explicitly computed by

$$Q\left(\frac{\kappa-\sigma^2 T N_{\rm RF}}{\sigma^2\sqrt{T N_{\rm RF}}}\right) = P_{\rm fa}, \tag{30}$$

where $Q(x) = \int_x^{+\infty} \frac{1}{\sqrt{2\pi}} e^{-\frac{x^2}{2}} dx$ is the Gaussian Q function. After some mathematical derivations, we can get

$$\kappa = \sigma^2\sqrt{T N_{\rm RF}} Q^{-1}\left(P_{\rm fa}\right) + \sigma^2 T N_{\rm RF}. \tag{31}$$

Hence, the algorithm terminates when $\|\bar{\mathbf{y}}_r\|^2 < \kappa$.

D. Near-field Channel Reconstruction

When the N-NOMP algorithm terminates, by applying the estimated ternary parameter sets, the uplink near-field channel can be reconstructed as

$$\hat{\mathbf{h}} = \sum_{l=1}^{\hat{L}} \hat{g}_l'' \mathbf{w}\left(\hat{\theta}_l'', \hat{r}_l''\right), \tag{32}$$

where $\hat{L}$ denotes the number of paths detected by the N-NOMP algorithm.

E. User Localization

The user location can be estimated from the channel parameters. When the LoS path exists, it has the maximum gain than any other path. When the LoS path does not exist, the reflected path has the maximum gain. The strongest path can be obtained in the first iteration of the N-NOMP algorithm as following

$$\left(\theta_{\rm energy}, r_{\rm energy}\right) = \left(\hat{\theta}_1'', \hat{r}_1''\right). \tag{33}$$

1) LoS path existence detection: When the maximum energy path is obtained, we need to determine whether it is a LoS path before estimating the user position.

As shown in Fig. 4, the minimum angle of reflected path is $\varphi_{\min}$, and the cosine of $\varphi_{\min}$ is $\theta_{\min} = \cos\left(\varphi_{\min}\right)$. If the maximum power path $\left(\theta_{\rm energy}, r_{\rm energy}\right)$ is a reflection path, the distance between the reference antenna and the image of the user $r_{\rm energy}$ should be greater than the minimum mirror distance in this direction $d_{\rm energy} = -\frac{(N-1)d+2S}{2\theta_{\rm energy}}$. Hence, the existence of LoS can be detected as follows:

$$\hat{\xi} = \begin{cases} 0, & \theta_{\rm energy} \le \theta_{\min} \text{ and } \mathrm{r}_{\rm energy} \ge \mathrm{d}_{\rm energy} \\ 1, & \text{else} \end{cases}. \tag{34}$$

If $\hat{\xi} = 1$, then we deduce that the LoS path exists and the detected strongest path is the LoS path, and the path parameters can be directly used to locate the user. If $\hat{\xi} = 0$, then the detected strongest path is a reflected path, and the path parameters need to be calculated using geometric reflection relations.

2) User Localization: The user position can be tracked by the following formula if the obtained maximum energy path is LoS:

$$\begin{cases} x_{\rm user} = r_{\rm energy}\sin(\cos^{-1}(\theta_{\rm energy})) \\ y_{\rm user} = -r_{\rm energy}\theta_{\rm energy} \end{cases}. \tag{35}$$

Otherwise, the user localization can be realized utilizing the geometric relationship between the reflection path parameters and the user location parameters as follows:

$$\begin{cases} x_{\rm user} = r_{\rm energy}\sin(\cos^{-1}(\theta_{\rm energy})) \\ y_{\rm user} = (N-1)\,d + 2S + r_{\rm energy}\theta_{\rm energy} \end{cases}. \tag{36}$$

IV. Evaluation Of The Reconstruction Channel

To evaluate the performance of the proposed channel reconstruction and user location scheme, simulations are carried out to evaluate the NMSE performance of the reconstructed channel at different system settings, i.e.

$$\mathrm{NMSE} = \mathrm{E}\left(\frac{\left\|\hat{\mathbf{h}}-\mathbf{h}\right\|^2}{\|\mathbf{h}\|^2}\right). \tag{37}$$

The carrier frequency is $f_c = 30$ GHz. The numbers of BS antennas and RF chains are $N = 256$ and $N_{\rm RF} = 4$, respectively. The number of multipath components between the user and the BS is $L = 4$. The noise variance is -174 dBm. The number of pilots is $T = 32$, while $S = 0.3$ meters.

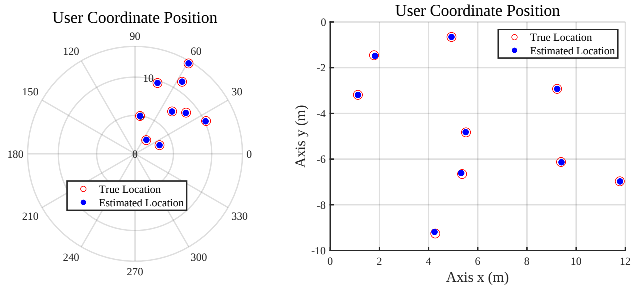

Fig. 6. User localization accuracy when the LoS path exists.

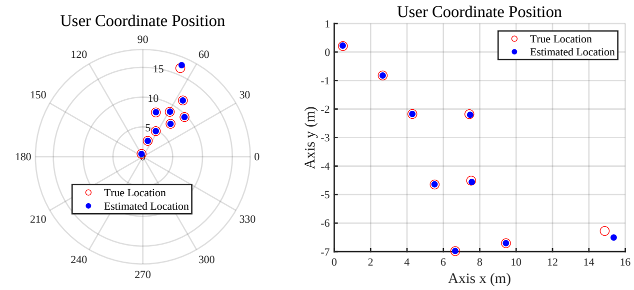

Fig. 7. User localization accuracy when the LoS path does not exist.

The angles θ_l are randomly generated from $(-1, 1)$ and the average distances between the user and the reference antenna at the BS is 10 meters.

The performance of the proposed N-NOMP algorithm for near-field channel estimation is compared with the traditional far-field channel estimation algorithm in [6] and the Fresnel-field channel estimation algorithm in [8]. As shown in Fig. 5, the proposed channel construction scheme has much better NMSE performance than other algorithms, and the performance is further improved with the increase of the SNR. This is because the proposed algorithm is built on the channel model that describes the deviations of both amplitude and phase among antennas, which is more comprehensive than the Fresnel-field and the far-field channel models.

The performance of the user localization algorithm when LoS path exists is shown in Fig. 6, where the average transmit power is -80 dBm. The results show that the detected user positions are very close to the real positions when the LoS exists. The localization algorithm can accurately determine the existence of the LoS path and locate users according to the LoS path parameters.

Finally, the localization algorithm is applied to the case where the LoS path does not exist and is blocked by obstacles between the user and the BS. Figure. 7 shows that the localization algorithm can still locate the user positions in the absence of LoS paths and has a high positioning accuracy, demonstrating the robustness of the proposed positioning scheme. Compared with the scenario with LoS path, the user positioning accuracy based on the reflecting path degrades slightly, which is mainly caused by the lower path power of the reflection path whose parameter detection is more susceptible to noise.

V. Conclusion

In this paper, a realistic near-field channel model, under which we proposed the phase and amplitude deviations among the receiving antennas was introduced and the proposed N-NOMP algorithm was utilized in the estimation of the near-field channel in an ELAA system which employs a subarray hybrid precoding architecture at the BS. A user localization algorithm was also proposed given some environment information. Based on the sparsity of the near-field channel in the joint angle-distance domain, the N-NOMP algorithm estimated and refined the multipath channel parameters using a limited amount of pilots and realized channel reconstruction. The user localization algorithm can determine the existence of LoS path and find the user position. Simulation results demonstrated that the proposed scheme can accurately reconstruct the near-field channel with low pilot cost and realize user localization with high precision whenever a LoS path exists or not.

VI. Acknowledgement

This work was supported in part by the National Natural Science Foundation of China (NSFC) under Grants 61941104, 61921004, and the Fundamental Research Funds for the Central Universities 2242022k3000x. The work of M. Matthaiou was supported by the European Research Council (ERC) under the European Union's Horizon 2020 research and innovation programme (grant agreement No. 101001331).

References

[1] M. Xiao, et al, "Millimeter wave communications for future mobile networks," *IEEE J. Sel. Areas Commun*, vol. 35, no. 9, pp. 1909–1935, Sept. 2017.

[2] M. Matthaiou, O. Yurduseven, H. Q. Ngo, D. Morales-Jimenez, S. L. Cotton, and V. F. Fusco, "The road to 6G: Ten physical layer challenges for communications engineers," *IEEE Commun. Mag*, vol. 59, no. 1, pp. 64-69, Jan. 2021.

[3] E. Björnson, Z. T. Demir, and L. Sanguinetti, "A primer on near-field beamforming for arrays and reconfigurable intelligent surfaces," *in Proc. IEEE ASILOMAR*, Nov. 2021.

[4] T. S. Rappaport, et al, "Wireless communications and applications above 100 GHz: Opportunities and challenges for 6G and beyond," *IEEE Access*, vol. 7, pp. 729–757, Jun. 2019.

[5] B. Ning, Z. Tian, Z. Chen, C. Han, J. Yuan, and S. Li, "Prospective beamforming technologies for ultra-massive MIMO in terahertz communications: A tutorial," 2021, *arXiv:2107.03032*.

[6] Y. Han, T. H. Hsu, C. -K. Wen, K. -K. Wong, and S. Jin, "Efficient downlink channel reconstruction for FDD multi-antenna systems," *IEEE Trans. Wireless Commun*, vol. 18, no. 6, pp. 3161-3176, Jun. 2019.

[7] Y. Han, Q. Liu, C. -K. Wen, M. Matthaiou, and X. Ma, "Tracking FDD massive MIMO downlink channels by exploiting delay and angular reciprocity," *IEEE J. Sel. Top. Signal Process*, vol. 13, no. 5, pp. 1062-1076, Sept. 2019.

[8] M. Cui, and L. Dai, "Channel estimation for extremely large-scale MIMO: Far-field or near-field?" 2021, *arXiv:2018.07581*.

[9] B. Mamandipoor, D. Ramasamy, and U. Madhow, "Newtonized orthogonal matching pursuit: Frequency estimation over the continuum," *IEEE Trans. Signal Process*, vol. 64, no. 19, pp. 5066-5081, Oct. 2016.

[10] Y. Zhu, H. Guo, and V. K. N. Lau, "Bayesian channel estimation in multi-user massive MIMO with extremely large antenna array," *IEEE Trans. Signal Process*, vol. 69, pp. 5463-5478, Sept. 2021.